

1 Barnaba: Software for Analysis of 2 Nucleic Acids Structures and 3 Trajectories

4 **Sandro Bottaro**^{1,2*}, **Giovanni Bussi**^{2*}, **Giovanni Pinamonti**^{2,3}, **Sabine**
5 **ReiBer**², **Wouter Boomsma**⁴, **Kresten Lindorff-Larsen**¹

***For correspondence:**

sandro.bottaro@bio.ku.dk
(SB); bussi@sissa.it (GB)

6 ¹Structural Biology and NMR Laboratory and Linderstrøm-Lang Centre for
7 Protein Science, Department of Biology, University of Copenhagen,
8 Copenhagen, Denmark; ²International School for Advanced Studies,
9 Trieste, Italy; ³Department of Mathematics and Computer Science, Freie
10 Universität, Berlin, Germany; ⁴Department of Computer Science,
11 University of Copenhagen, Copenhagen, Denmark

12

13 **Abstract** RNA molecules are highly dynamic systems characterized by a
14 complex interplay between sequence, structure, dynamics, and function.
15 Molecular simulations can potentially provide powerful insights into the nature of
16 these relationships. The analysis of structures and molecular trajectories of
17 nucleic acids can be non-trivial because it requires processing very
18 high-dimensional data that are not easy to visualize and interpret.
19 Here we introduce Barnaba, a Python library aimed at facilitating the analysis of
20 nucleic acids structures and molecular simulations. The software consists of a
21 variety of analysis tools that allow the user to i) calculate distances between
22 three-dimensional structures using different metrics, ii) back-calculate
23 experimental data from three-dimensional structures, iii) perform cluster analysis
24 and dimensionality reductions, iv) search three-dimensional motifs in PDB
25 structures and trajectories and v) construct elastic network models (ENM) for
26 nucleic acids and nucleic acids-protein complexes.
27 In addition, Barnaba makes it possible to calculate torsion angles, pucker
28 conformations and to detect base-pairing/base-stacking interactions. Barnaba
29 produces graphics that conveniently visualize both extended secondary structure
30 and dynamics for a set of molecular conformations. Barnaba is available as a
31 command-line tool as well as a library, and supports a variety of file formats such
32 as PDB, dcd and xtc files. Source code, documentation and examples are freely
33 available at <https://github.com/srnas/barnaba> under GNU GPLv3 license.

34

35 Introduction

36 Despite their simple four-letters alphabet, RNA molecules can adopt amazingly
37 complex three-dimensional architectures. RNA structure is often described in
38 terms of few, simple degrees of freedom such as backbone torsion angles,
39 sugar puckering, base-base interactions, and helical parameters *Dickerson (1989);*
40 *Richardson et al. (2008)*. Given a known three-dimensional structure, the cal-
41 culation of these properties can be performed using available tools such as
42 MC-annotate *Gendron et al. (2001)*, 3DNA *Lu and Olson (2008)*, fr3D *Sarver et al.*
43 *(2008)* or DSSR *Lu et al. (2015)*. These software packages make it possible to
44 calculate a variety of structural properties, but are less suitable for analyzing and
45 comparing large numbers of structures.

46 The lack of large-scale analysis tools is critical when considering that many
47 RNA molecules are not static, but highly dynamic entities, and multiple confor-
48 mations are required to describe their properties. In molecular dynamics (MD)
49 simulations *Šponer et al. (2018)*, for example, it is often necessary to analyze
50 several hundreds of thousands of structures. The analysis and comparison of
51 results from structure-prediction algorithms poses similar challenges *Dawson and*
52 *Bujnicki (2016); Miao et al. (2017)*. In order to rationalize and generate scientific
53 insights, it is therefore fundamental to employ specific analysis and visualization
54 tools that can handle such highly-dimensional data. This need has been long
55 recognized in the field of protein simulations, leading to the development of
56 several software packages for the analysis of MD trajectories *Michaud-Agrawal*
57 *et al. (2011); McGibbon et al. (2015); Tiberti et al. (2015)*. While these software
58 can be in principle used to analyze generic simulations, they do not support the
59 calculation of nucleic-acids-specific quantities out of the box. Notable exceptions
60 are CPPTRAJ *Roe and Cheatham III (2013)*, and the driver tool in PLUMED *Tribello*
61 *et al. (2014)*, that support the calculation of nucleic acids structural properties,
62 among other features.

63 A limited number of software packages have been developed with the main
64 purpose of analyzing simulations of nucleic acids. Curves+ *Lavery et al. (2009)*
65 calculates parameters in DNA/RNA double helices as well as torsion backbone
66 angles. *do_{x3dna}* *Kumar and Grubmüller (2015)* extends the capability of the 3DNA
67 package to analyze few selected quantities from GROMACS *Abraham et al. (2015)*
68 MD trajectories. The detection of hydrogen bonds/stacking in simulations and the
69 identification of motifs such as helices, junctions, loops, etc. can be performed
70 using the Motif Identifier for Nucleic acids Trajectory (MINT) software *Górska et al.*
71 *(2015)*.

72 Here we present Barnaba, a Python library to analyze nucleic acids structures
73 and trajectories. The library contains routines to calculate various structural pa-
74 rameters (e.g. distances, torsion angles, base-pair and base-stacking detection), to

75 perform dimensionality reduction and clustering, to back-calculate experimental
76 quantities from structures and to construct elastic network models. Barnaba
77 utilizes the capabilities of MDTraj *McGibbon et al. (2015)* for reading/writing tra-
78 jectory files, and thus supports many different formats, including PDB, dcd, xtc,
79 and trr.

80 In this paper we show the capabilities of Barnaba by analyzing a long MD
81 simulation of an RNA stem-loop structure. We first calculate distances from a
82 reference frame. Second, we consider a subset of dihedral angles and compare
83 3J scalar couplings calculated from simulations with nuclear magnetic resonance
84 (NMR) data. We then perform a cluster analysis of the trajectory, identifying
85 a number of clusters that are visualized using a dynamic secondary structure
86 representation. Finally, we search for structural motifs similar to cluster centroids
87 in the entire protein data bank (PDB) database. In addition, we show how to
88 construct an elastic network model (ENM) of RNA molecules and protein-nucleic
89 acid complexes with Barnaba, and how to use it to estimate RNA local fluctuations.

90 Results

91 We present the different features of Barnaba by analyzing a 180 μ s long simulation
92 of an RNA 14-mers with sequence GGCACUUCGGUGCC performed by Tan et al. *Tan*
93 *et al. (2018)* using a simulated tempering protocol where the temperature is used
94 as a dynamic variable to enhance sampling. Experimentally, this sequence is
95 known to form an A-form stem composed by 5 consecutive Watson-Crick base
96 pairs, capped by a UUCG tetraloop (Fig. 1A).

97 RMSD, eRMSD calculation and detection of base-base interactions.

98 First, we calculate the distance of each frame in the simulation from the reference
99 experimental structure (PDB code 2KOC *Nozinovic et al. (2010)*). Fig.1B shows
100 the time series of heavy-atom root mean squared distance (RMSD) after optimal
101 superposition *Kabsch (1976)*. During this simulation, multiple folding events occur:
102 In line with previous analyses *Tan et al. (2018)* we thus observe both structures
103 close to the reference as well as unfolded/misfolded ones.

104 We identify the base-base interactions in each frame using the annotation
105 functionality in Barnaba (see Methods). Structures where the stem is completely
106 formed together with the native trans sugar-Watson (tSW) interaction between
107 U6-G9 in the loop are shown in red. Blue points indicate structures in which all
108 base pairs in the stem, but not in the loop, are present. All the other structures are
109 colored in gray. From the histogram in Fig. 1B it can be seen that RMSD < 0.23nm
110 roughly corresponds to native-like structures. A second sharp peak around 0.3nm
111 corresponds to structures in which only the stem is correctly formed. All other
112 conformations have RMSD larger than 0.6nm.

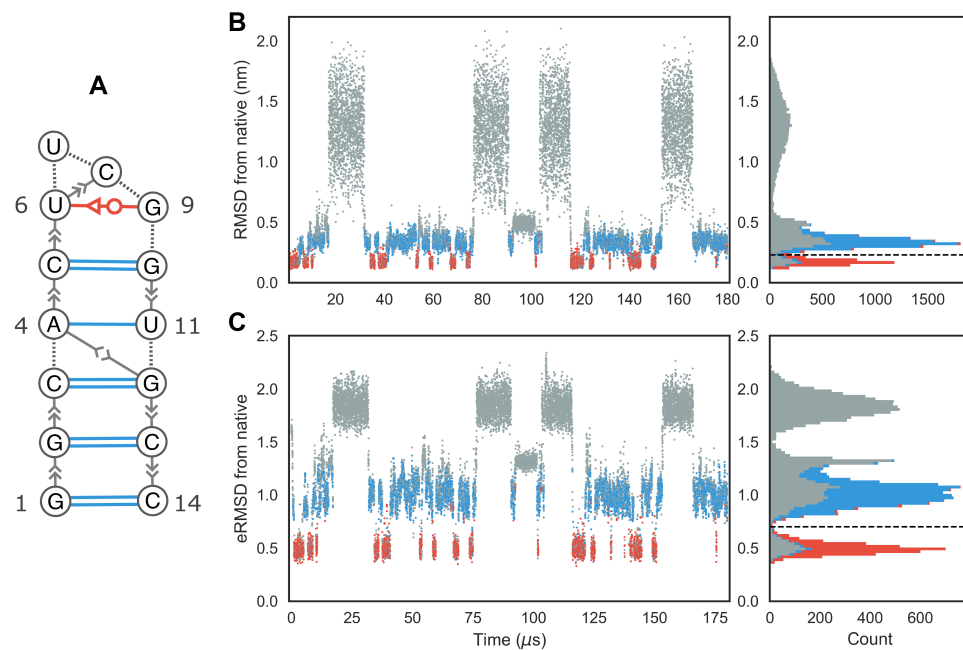


Figure 1. **A)** Extended secondary structure representation of the UUCG stem-loop. Watson-Crick base pairs are shown in blue, trans Sugar-Watson base pair between U6 and G9 is shown in red. **B)** RMSD from native over time of the UUCG simulation. The corresponding histogram is shown in the right panel. The dashed line at RMSD=0.23nm separates native-like from non-native-like structures. The colors indicate the presence of native base-base interactions, as shown in the secondary structure representation. Structures where all Watson-Crick interactions in the stem and the trans Sugar-Watson base pair in loop is formed are shown in red. Blue indicates structures where only the stem is formed. All other conformations are shown in gray. **C)** eRMSD from native structure over time. Color scheme is identical to panel **B**. Dashed line at eRMSD=0.7 separates native-like from non-native conformations.

113 One of the feature of Barnaba is the possibility to calculate the eRMSD **Bottaro**
114 **et al. (2014)**. The eRMSD only considers the relative arrangements between nu-
115 cleobases in a molecule, and quantifies the differences in the interaction network
116 between two structures. In this perspective, eRMSD is similar to the Interaction
117 Fidelity Network **Parisien et al. (2009)** that quantifies the discrepancy in the set of
118 base-pairs and base-stacking interactions. The eRMSD, however, is a continuous,
119 symmetric, positive definite metric distance that satisfies the triangular inequality.
120 Additionally, it does not require detection of the interactions (annotation) and is
121 hence particularly well suited for analyzing MD trajectories and unstructured RNA
122 molecules. Fig.1C shows the eRMSD from native for the UUCG simulation. We
123 notice that, similarly to the RMSD case, the histogram displays three main peaks.
124 In this case the correspondence between peaks and structures can be readily
125 identified: when $eRMSD < 0.7$ native stem and loop are formed, if $0.7 < eRMSD < 1.3$,
126 stem is formed but the loop is in a non-native configuration. Other structures
127 typically have $eRMSD > 1.3$. We observe that the separation between the two main
128 peaks (native structure, red, and native stem, blue) is sharper in Fig.1C, confirming
129 that eRMSD is more suitable than RMSD to distinguish structures with different
130 base pairings **Bottaro et al. (2014)**.

131 Note that a significant number of low-RMSD/eRMSD structures lack one or
132 more native base-pair interactions, and are therefore shown in gray. This is
133 because the detection of base-base interactions critically depends on a set of
134 geometrical parameters (e.g. distance, base-base orientation, etc.) that were
135 calibrated on high-resolution structures. The criteria used in Barnaba (as well as
136 the ones employed in other annotation tools) may not always be accurate when
137 considering intermediate states and partially formed interactions that are often
138 observed in molecular simulations **Lemieux and Major (2002)**.

139 **Torsion angle and 3J scalar coupling calculations**

140 Another important class of structural parameters is torsion angles. Similarly to
141 other software, Barnaba contains routines to calculate backbone torsion angles
142 ($\alpha, \beta, \gamma, \delta, \epsilon, \zeta$), the glycosidic angle χ , and the pseudorotation sugar parameters
143 **Altona and Sundaralingam (1972)**.

144 In Fig. 2, left panels we plot the probability distributions of four angles (β, γ, δ
145 and ϵ) for three different residues: U6, U7, and G9. We can see from the dis-
146 tribution of γ angles that U6 and U7 mainly populate the *gauche*⁺ rotameric
147 state ($0^\circ < \gamma \leq 120^\circ$), while G9 significantly populates the *trans* state as well
148 ($120^\circ < \gamma \leq 240^\circ$). Different rotameric states can be also seen from the distribution
149 of δ angles (C2'/C3'-endo) and ϵ , that is related to BI/BII states. Here, we consider
150 the same trajectory of the UUCG tetraloops described above and removed all the
151 unfolded structures, i.e. structures with eRMSD from native larger than 1.5 (\approx
152 6000 out of 20000), because we below compare to experiments under conditions

153 where these are absent.

154 In this example we chose these specific torsion angles because their distribu-
155 tion is related to available 3J couplings experimental data from nuclear magnetic
156 resonance (NMR) spectroscopy. The magnitude of 3J coupling depends on the dis-
157 tance between atoms connected by three bonds, and thus on the corresponding
158 dihedral angle distribution. The dependence between angle θ and coupling 3J
159 can be calculated via Karplus equations $^3J = A \cos^2(\theta + \phi) + B \cos(\theta + \phi) + C$, where
160 A, B, C are empirical parameters. Couplings corresponding to different angles can
161 be calculated with Barnaba. H1'-H2', H2'-H3', H3'-H4' (sugar conformation), H5'-P,
162 H5''-P, C4-P (β), H4'-H5', H4'-H5'' (γ), H3-P(+1), C4-P(+1) (ϵ), H1'-C8/C6, and H1'-C4/C2
163 (χ). The complete list of Karplus parameters is reported in the Methods section,
164 and may be changed within Barnaba.

165 Fig. 2, right panels, show the back-calculated average 3J couplings and the
166 corresponding experimental value reported in *Nozinovic et al. (2010)*. Note that
167 in some cases experiments and simulations do not agree: this is because the
168 simulation was performed at different temperatures using a simulated tempering
169 protocol, and therefore the comparison between simulations and experiments is
170 here made for illustrative purposes only. Significant discrepancies could originate
171 from errors introduced by the Karplus equations, that can be as large as 2Hz
172 *Bottaro et al. (2018)*.

173 Cluster analysis

174 The structures within a trajectory can be grouped into clusters of mutually similar
175 conformations, to understand which different states are visited and how often.
176 For clustering we use the DBSCAN *Ester et al. (1996)* algorithm with $\epsilon = 0.45$ and
177 min samples=70 *Bottaro and Lindorff-Larsen (2017)*. As in the previous example,
178 structures with eRMSD > 1.5 from native are discarded. Figure 3A shows the
179 trajectory projected onto the first two components of a principal component
180 analysis done on the collection of G-vectors *Bottaro and Lindorff-Larsen (2017)*.
181 Circles show the resulting 9 clusters, whose radius is proportional to the square
182 root of their size. The 5500 structures (40%) that were not assigned to any cluster
183 are shown as gray dots. For each cluster we identify its centroid, here defined as
184 the structure with the lowest average distance from all other cluster members.

185 Ideally, clusters should be compact enough so that the centroid can be consid-
186 ered as a representative structure. This information is shown in the box-plot in Fig.
187 3B, that reports the distances (eRMSD and RMSD, as labeled) between centroids
188 and cluster members. At the same time, structures within clusters are not all
189 identical to one another. In order to visualize the intra-cluster variability we have
190 found it useful to introduce a “dynamic secondary structure” representation. In
191 essence, we detect base-stacking/base-pair interactions in all structures within a
192 cluster, and calculate the fraction of frames in which each interaction is present.

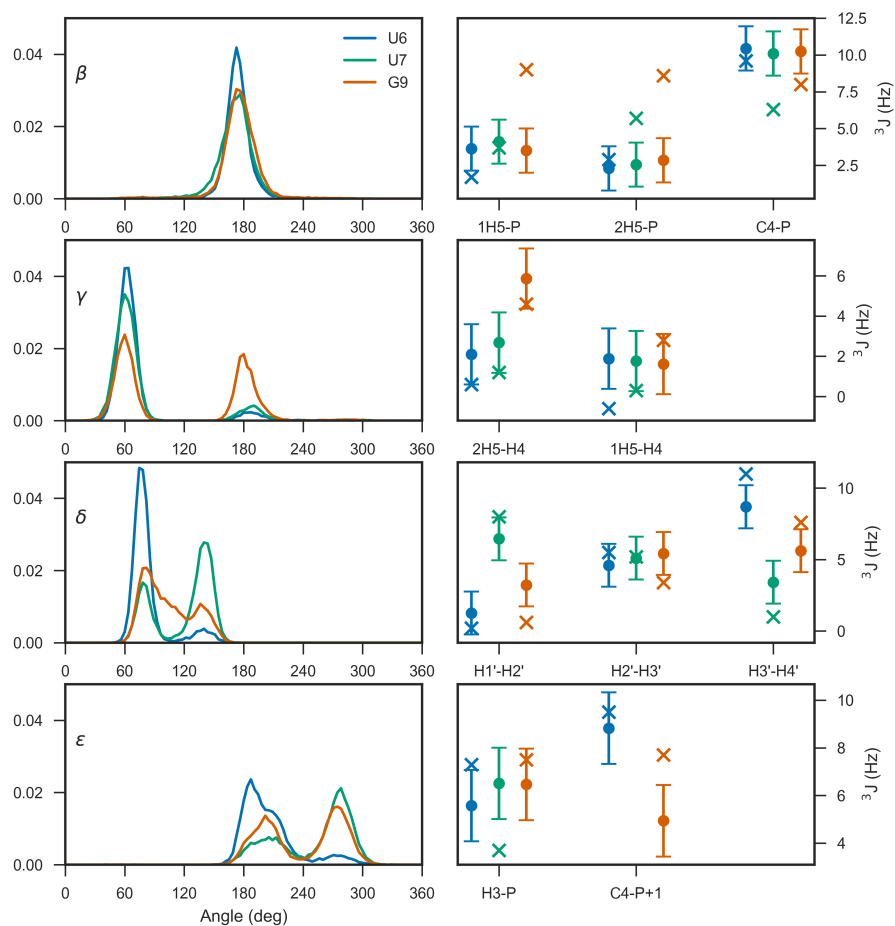


Figure 2. Left panels: Torsion angle distribution for β, γ, δ and ϵ in residues U6, U7, and G9. Right panels show the experimental 3J couplings (crosses) and the calculated value from simulation (dots). The error bars indicate the standard error of the mean calculated over 4 blocks.

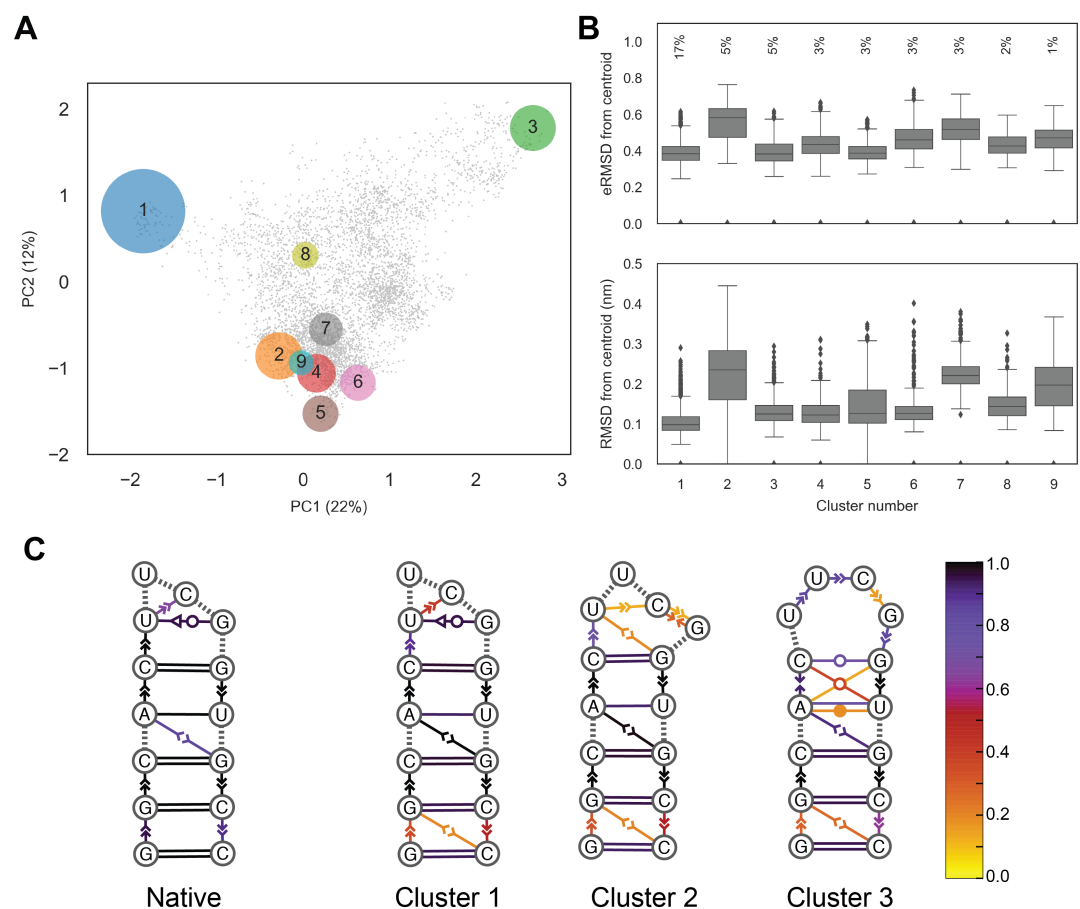


Figure 3. Example of a cluster analysis on the UUCG stem-loop trajectory. **A**) principal component analysis on the collection of G-vectors *Bottaro and Lindorff-Larsen (2017)*. Each circle corresponds to a cluster, gray dots show unassigned structures. Circles are centered in the centroid positions, and the radii are proportional to the square root of the population. The percentage of explained variance of the first two components is indicated on the axes. **B**) Box-plots reporting eRMSD (top) and RMSD (bottom) from cluster centroids. Lower/upper hinges correspond to the first and third quartiles, while whiskers indicate lowest/highest data within 1.5 interquartile range. Data beyond the end of the whiskers are shown individually. The percentages indicate the cluster population. **C**) Dynamic secondary structure representation of the 20 native NMR conformers (PDB 2KOC) and of the first three clusters. The extended secondary structure annotation follows the Leontis-Westhof classification. The color scheme shows the fraction of frames within a cluster for which the interaction is formed.

193 The population of each interaction is shown by coloring the extended secondary
194 structure representation (Fig.3C). This representation has some analogy with the
195 “dot plot” representation used to display secondary structure ensembles obtained
196 using nearest neighbor models, that reports the predicted probability of individual
197 base pairs *Jacobson and Zuker (1993)*. We can see that the first three clusters
198 correspond to three different tetraloop structures. In cluster 1, the U6-G9 tSW
199 base pair is present, together with the U6-C8 stacking typical of the native UUCG
200 tetraloop structure. In cluster 2, no U6-G9 base pair is present, while in cluster 3
201 we observe stacking between U6-U7-C8-G9, as also described in the next section.
202 In all clusters the population of the terminal base pairs and stacking is lower than
203 one, indicating the presence of base fraying.

204 In our experience, cluster analysis is useful to understand and visualize quali-
205 tatively the different type of structures in a simulation. In many practical cases,
206 however, the number of clusters and their population may differ depending on
207 the employed clustering algorithm and associated parameters. Clustering may
208 not even be meaningful when considering highly unstructured systems such as
209 long single-stranded nucleic acids lacking secondary structures *Chen et al. (2012)*.

210 **Motif search**

211 Barnaba can be used to search for structural motifs in a PDB file or trajectory
212 using the eRMSD distance. In the following example, we illustrate this feature
213 by taking the centroids of the first three clusters described above and search for
214 similar structures within the PDB database. In order to focus on the loop structure,
215 rather than on stem variability, we consider the tetraloop and the two closing
216 base pairs for the search (residues 4-11 in Fig.1A). The search is performed
217 against all RNA-containing structures in the PDB database (retrieved May 4th,
218 2018, resolution 3.5Å or better). The database considered here consists of 3067
219 X-ray, 652 NMR and 177 cryo electron-microscopy (EM) structures. Note that the
220 search is purely based on the geometrical arrangement of nucleobases, without
221 restriction on the sequence, a particular feature that is also enabled by the use of
222 eRMSD.

223 Figure 4 shows the cluster centroids (gray) and the closest motif match, i.e. the
224 lowest eRMSD substructure in the PDB database (orange). The eRMSD between
225 the cluster centroid and the best match are indicated, together with the associated
226 PDB code. Centroid 1 corresponds to the canonical UUCG tetraloop structure, with
227 the signature tSW interaction between U6-G9 and G9 in syn conformation. Note
228 that the eRMSD between centroid and best match is small (0.25), indicating that
229 simulated and experimental structures are highly similar. Cluster 2 corresponds
230 to a structure in which the stem is formed, C8 is stacked on top of U6 and G9 is
231 bulged out. Centroid 3 features four consecutive stacking between U6-U7-C8-G9.
232 Note that this latter structure is remarkably similar to the 4-stack loop described

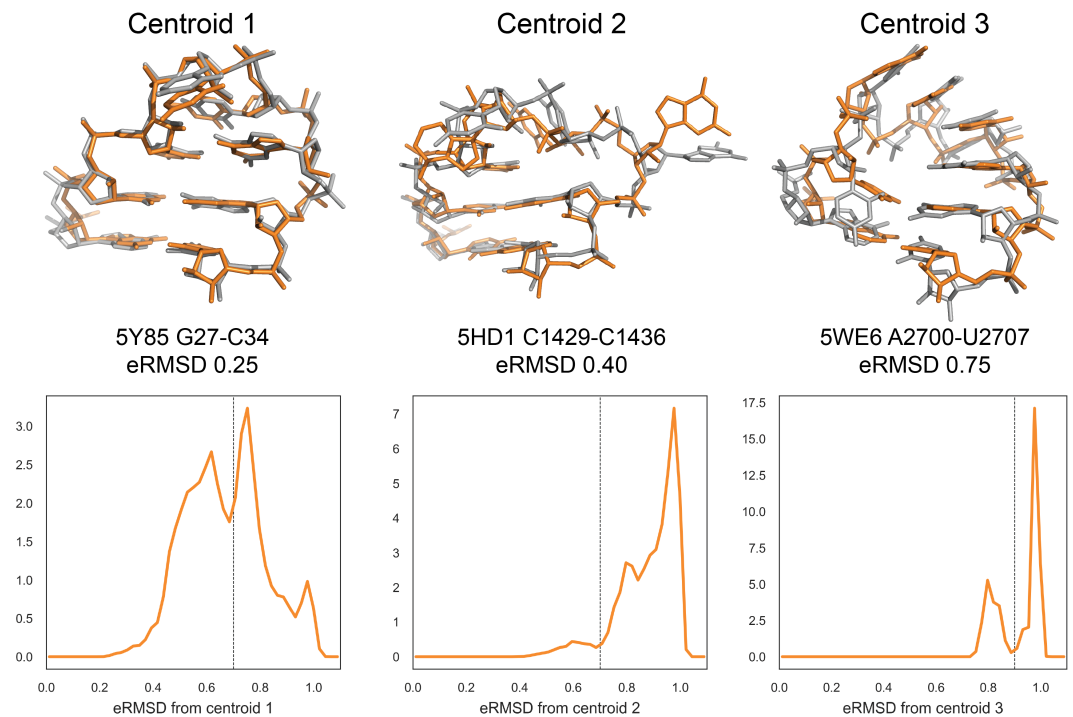


Figure 4. Motif search in PDB database. Top panels: centroids of the first three clusters (in gray) superimposed on the closest structures from the PDB database (orange). eRMSD between centroid and the best match are indicated, together with the associated PDB code. Bottom panels: eRMSD distribution between centroid and substructures from PDB database. Note that different distributions are obtained for different clusters, meaning that the eRMSD threshold varies depending on the motif. Distances larger than eRMSD=1 are not reported. The eRMSD threshold at 0.7 (centroids 1,2) and 0.9 (centroid 3) is indicated as a dashed line.

233 in *Bottaro and Lindorff-Larsen (2017)*.

234 As a rule of thumb, we consider as significant matches structures below 0.7
235 eRMSD, but there are cases in which it is worth considering structures in the
236 0.7-1.0 eRMSD range as well. More generally, it is useful to consider the histogram
237 of all fragments with eRMSD below 1, as shown in Fig. 4, bottom panels. This type
238 of analysis makes it possible to identify a good threshold value, in correspondence
239 to minima in the probability distributions. For example, there are no structures
240 in the PDB with eRMSD lower than 0.7 for centroid 3. In this case, a value of 0.9
241 should be used instead.

242 In this example we performed a simple search of a structure from simulation
243 against experimentally-derived structures downloaded from the PDB database.
244 In Barnaba, any arbitrary motif can be used as a query by providing a coordinate
245 file with at least the position of C2,C4 and C6 atoms for each nucleotide. Searches
246 with more complex motifs composed by two strands (e.g. K-turns, sarcin-ricin
247 motifs, etc.) are also possible. Additionally, Barnaba allows for inserted bases,
248 thereby identifying structural motifs with one or more bulged-out bases.

249 **Elastic Network Models**

250 Elastic Network Models (ENMs) are minimal computational models able to capture
251 the dynamics of macromolecules at a small computational cost. They assume that
252 the system can be represented as a set of beads connected by harmonic springs,
253 each having rest length equal to the distance between the two beads it connects,
254 in a reference structure (usually, an experimental structure from the PDB). First
255 introduced to analyze protein dynamics *Tirion (1996)*, ENMs are also applicable
256 to structured RNA molecules *Bahar and Jernigan (1998)*; *Setny and Zacharias*
257 *(2013)*; *Zimmermann and Jernigan (2014)*. Barnaba contains routines to construct
258 ENM of nucleic acids and proteins, and, as unique feature, makes it possible
259 to calculate fluctuations between consecutive C2-C2 atoms. In a previous work
260 *Pinamonti et al. (2015)*, we have shown this quantity to correlate with flexibility
261 measurements performed with selective 2-hydroxyl acylation analyzed by primer
262 extension (SHAPE) experiments *Merino et al. (2005)*. Here, we show an example
263 of ENM analysis on two RNA molecules: the 174-nucleotide sensing domain of
264 the *Thermotoga maritima* lysine riboswitch (PDB ID: 3DIG), and the *Escherichia*
265 *coli* 5S rRNA (PDB ID: 1C2X). We construct an all-atom ENM (AA-ENM), where each
266 heavy atom is a bead, together with a cutoff radius of 7 Å. In figure 5 we show
267 the flexibility of the RNA molecules as predicted by the ENM (black), that can be
268 qualitatively compared with the measured SHAPE reactivity *Hajdin et al. (2013)*
269 (orange).

270 The implementation of the ENM in Barnaba employs the sparse matrix pack-
271 age available in Scipy, that allows for significant speed-ups compared to the
272 dense-matrix implementation. Fig. 6 shows the execution time for constructing

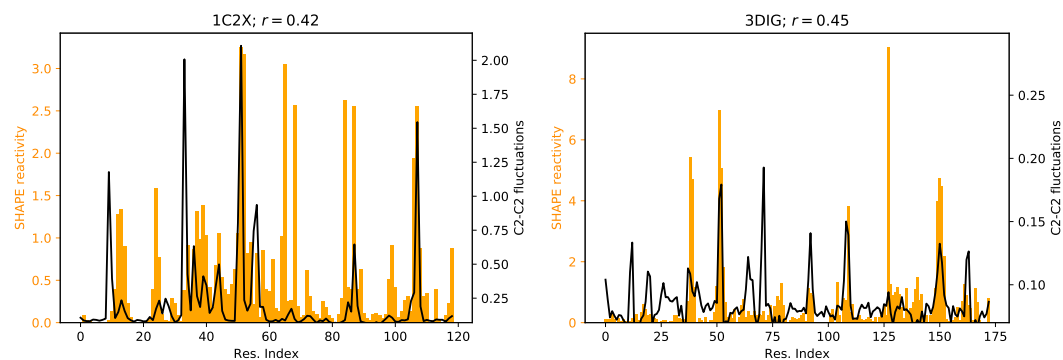


Figure 5. C2-C2 fluctuations as predicted by the ENM of Lysine riboswitch (right panel) and 5S rRNA (left panel). SHAPE reactivity data from *Hajdin et al. (2013)* are shown for comparison. Pearson correlation coefficient r between SHAPE data and ENM-predicted fluctuations is also indicated.

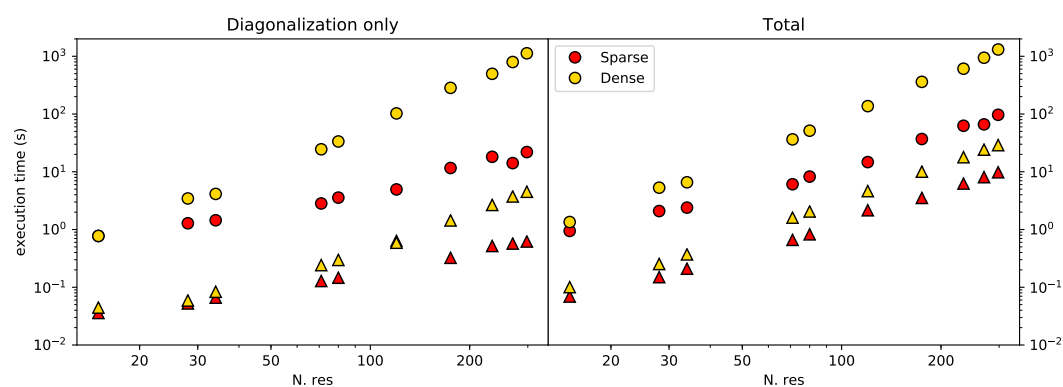


Figure 6. Execution time for the ENM calculation using sparse matrices (yellow) or dense matrices (red) on a 2.3 GHz Dual-Core Intel Core i5 processor, as a function of the number of residues in the RNA molecule. Results are shown both for sugar-base-phosphate (SBP) ENM (triangles) and all-atom-ENM (AA-ENM) (circles), as defined in *Pinamonti et al. (2015)*. Left panel shows the time for the interaction matrix diagonalization only, right panel shows the total time including the calculation of C2-C2 fluctuations.

273 ENMs (both SBP and AA) of biomolecules with sizes ranging from a few tens to
274 several hundreds nucleotides. Calculations were performed running Barnaba on
275 a personal computer. This, combined with the significant memory saving granted
276 by sparse matrices representation, makes it possible to easily compute the vi-
277 brational modes and the local flexibility of large RNA systems such as ribosomal
278 structures using a limited amount of computer resources.

279 Discussion

280 Many RNA molecules are highly dynamical entities that undergo conformational
281 rearrangements during function. For this reason, it is becoming increasingly im-
282 portant to develop tools to analyze not only single structures, but also trajectories
283 (ensembles) obtained from molecular simulations. In this paper we introduce a
284 software to facilitate the analysis of nucleic acids simulations. The program, called
285 Barnaba, is available both as a Python library as well as a command line tool. The
286 output of the program is such that it can be easily used to calculate averages
287 and probability distributions, or conveniently used as input to the many existing
288 plotting and analysis libraries (e.g. Matplotlib, SKlearn) available in Python.

289 Barnaba consists of a number of functions: some of them implement standard
290 calculations (RMSD, torsion angles, base-pairs and base-stacking detection). A
291 unique feature of Barnaba is the possibility to calculate the eRMSD. This metric
292 has been successfully employed in several contexts: for analyzing MD simulations
293 *Kuhrova et al. (2016)*, as a biased collective variable in enhanced sampling simu-
294 lations *Bottaro et al. (2016)*; *Yang et al. (2017)*; *Poblete et al. (2018)*, to construct
295 Markov State models *Pinamonti et al. (2017)* and to cluster RNA tetraloop struc-
296 tures *Bottaro and Lindorff-Larsen (2017)*. In this paper we show the usefulness
297 of this metric to monitor simulations over time, to perform cluster analysis and to
298 search for structural motifs within trajectories/structures. This last feature can
299 be extremely useful to experimental structural biologists, as it makes it possible
300 to efficiently search for arbitrary query motifs within the entire PDB database.
301 For analyzing simulations and clusters, we have found it useful to introduce a
302 dynamic secondary structure representation, that recapitulates the variability of
303 base-pair and base-stacking interactions within an ensemble.

304 Another unique feature of Barnaba is the possibility to back-calculate 3J scalar
305 couplings from structures. This calculation is *per se* extremely simple. However, it
306 can be difficult to obtain from the literature the different sets of Karplus parame-
307 ters, and the calculation of the corresponding dihedral angles is error-prone.

308 Finally, Barnaba contains a routine to construct ENMs of nucleic acid and
309 protein systems and complexes. This is a useful, fast and computationally cheap
310 tool to predict the local dynamical properties of biomolecules, as well as the chain
311 flexibility of RNA molecules.

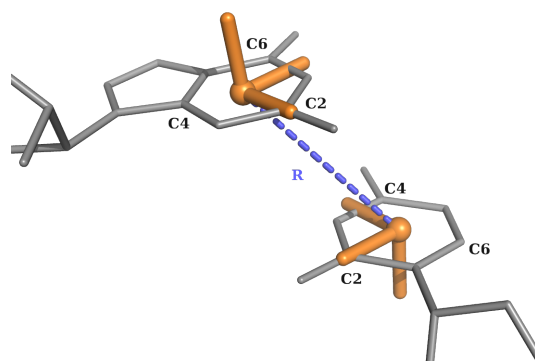


Figure 7. Definition of the local coordinate systems and of the vector \mathbf{R} for purines and pyrimidines.

312 **Methods and Materials**

313 **Implementation and availability**

314 Barnaba is a Python library and command line tool. It requires Python 2.7
315 or > 3.3, Numpy, and Scipy libraries. Additionally, Barnaba requires MDTraj
316 (<http://mdtraj.org/>) for manipulating structures and trajectories. Source code
317 is freely available at <https://github.com/srnas/barnaba> under GNU GPLv3 license.
318 The github repository contains documentation as well as a set of examples.

319 **Relative position and orientation of nucleobases**

320 For each nucleotide, a local coordinate system is set up in the center of C2, C4, and
321 C6 atoms. The x-axis points toward the C2 atom, and the y-axis in the direction
322 of C4 (C/U) or C6 (A/G). The origin of the coordinates of nucleobase j in the
323 reference system constructed on base i is the vector $\mathbf{R}_{ij} = \{x_{ij}, y_{ij}, z_{ij}\}$. Note that
324 $|\mathbf{R}_{ij}| = |\mathbf{R}_{ji}|$ but $\mathbf{R}_{ij} \neq \mathbf{R}_{ji}$. The \mathbf{R}_{ij} is central in the definition of the eRMSD metric
325 and of the annotation strategy described below.

326 **eRMSD**

327 The eRMSD is a contact-map based distance, with the addition of a number of
328 features that make it suitable for the comparison of nucleic acids structures. We
329 briefly describe here the procedure, originally introduced in *Bottaro et al. (2014)*.
330 Given a three-dimensional structure α , one calculates \mathbf{R}_{ij}^α for all pairs of bases in a
331 molecule. The position vectors are then rescaled as follows:

$$\tilde{\mathbf{r}}_{ij}^\alpha = \left(\frac{x_{ij}^\alpha}{a}, \frac{y_{ij}^\alpha}{a}, \frac{z_{ij}^\alpha}{b} \right) \quad (1)$$

332 with $a = 5\text{\AA}$ and $b = 3\text{\AA}$. The rescaling effectively introduces an ellipsoidal anisotropy
333 that is peculiar to base-base interactions. Given two structures, α and β , consisting

334 of N residues, the eRMSD is calculated as

$$eRMSD = \sqrt{\frac{1}{N} \sum_{i,j} |\mathbf{G}(\tilde{\mathbf{r}}_{ij}^{\alpha}) - \mathbf{G}(\tilde{\mathbf{r}}_{ij}^{\beta})|^2} \quad (2)$$

335 \mathbf{G} is a non-linear function of $\tilde{\mathbf{r}}$ defined as:

$$\mathbf{G}(\tilde{\mathbf{r}}) = \begin{pmatrix} \sin(\gamma\tilde{r}) \frac{\tilde{r}_x}{\tilde{r}} \\ \sin(\gamma\tilde{r}) \frac{\tilde{r}_y}{\tilde{r}} \\ \sin(\gamma\tilde{r}) \frac{\tilde{r}_z}{\tilde{r}} \\ 1 + \cos(\gamma\tilde{r}) \end{pmatrix} \times \frac{\Theta(\tilde{r}_{\text{cutoff}} - \tilde{r})}{\gamma} \quad (3)$$

336 where $\gamma = \pi/\tilde{r}_{\text{cutoff}}$ and Θ is the Heaviside step function. Note that the function \mathbf{G}
337 has the following desirable properties:

- 338 1. $|\mathbf{G}(\tilde{\mathbf{r}}^{\alpha}) - \mathbf{G}(\tilde{\mathbf{r}}^{\beta})| \approx |\tilde{\mathbf{r}}^{\alpha} - \tilde{\mathbf{r}}^{\beta}|$ if $\tilde{r}^{\alpha}, \tilde{r}^{\beta} \ll \tilde{r}_{\text{cutoff}}$.
- 339 2. $|\mathbf{G}(\tilde{\mathbf{r}}^{\alpha}) - \mathbf{G}(\tilde{\mathbf{r}}^{\beta})| = 0$ if $\tilde{r}^{\alpha}, \tilde{r}^{\beta} \geq \tilde{r}_{\text{cutoff}}$.
- 340 3. $\mathbf{G}(\tilde{\mathbf{r}})$ is a continuous function.

341 The cutoff value is set to $\tilde{r}_{\text{cutoff}} = 2.4$.

342 Annotation

343 A pair of bases i and j is considered for annotation only if $|\tilde{\mathbf{r}}_{ij}| < 1.7$ and $|\tilde{\mathbf{r}}_{ji}| < 1.7$.

344 **Stacking.** The criteria for base-stacking are the following:

$$(|z_{ij}| \text{ and } |z_{ji}| > 2\text{\AA}) \text{ and } (\rho_{ij} \text{ or } \rho_{ji} < 2.5\text{\AA}) \text{ and } (|\theta_{ij}| < 40^{\circ}) \quad (4)$$

345 Here, $\rho_{ij} = \sqrt{x_{ij}^2 + y_{ij}^2}$ and θ_{ij} is the angle between the vectors normal to the
346 planes of the two bases. Similarly to other annotation approaches **Gendron et al.**
347 **(2001)**; **Sarver et al. (2008)**; **Waleń et al. (2014)**, we identify four different classes
348 of stacking interactions according to the sign of the z coordinates:

- 349 • upward: ($>>$ or 3'-5') if $z_{ij} > 0$ and $z_{ji} < 0$
- 350 • downward: ($<<$ or 5'-3') if $z_{ij} < 0$ and $z_{ji} > 0$
- 351 • outward: ($<>$ or 5'-5') if $z_{ij} < 0$ and $z_{ji} < 0$
- 352 • inward: ($><$ or 3'-3') if $z_{ij} > 0$ and $z_{ji} > 0$

353 We notice that, with this choice, consecutive base pairs with alternating purines
354 and pyrimidines result in a cross-strand outward stacking (see, e.g., Figure 1A).

355 **Base-pairing.** Base-pairs are classified according to the Leontis-Westhof
356 nomenclature **Leontis and Westhof (2001)**, based on the observation that hy-
357 drogen bonding between RNA bases involve three distinct edges: Watson-Crick
358 (W), Hoogsteen edge (H), and sugar (S). An additional distinction is made accord-
359 ing to the orientation with respect to the glycosydic bonds, in cis (c) or trans (t)
360 orientation.

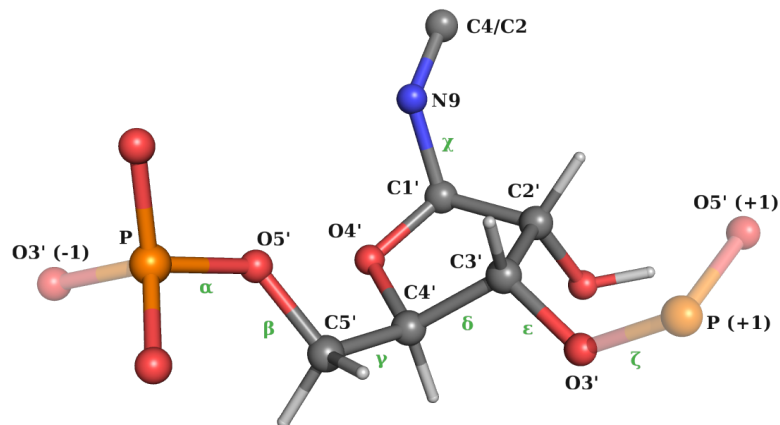


Figure 8. Definition of the backbone/glycosidic angles χ *Frellsen et al. (2009)*.

361 In Barnaba, all non-stacked bases are considered base-paired if $|\theta_{ij}| < 60^\circ$
362 and there exists at least one hydrogen bond, calculated as the number of donor-
363 acceptor pairs with distance $< 3.3\text{\AA}$. Edges are defined according to the value of
364 the angle $\psi = \arctan 2(\hat{y}_{ij}, \hat{x}_{ij})$.

- 365 • Watson-Crick edge (W): $0.16 < \psi \leq 2.0\text{rad}$
- 366 • Hoogsteen edge (H): $2.0 < \psi \leq 4.0\text{rad}$.
- 367 • Sugar edge (S): $\psi > 4.0\text{rad}, \psi \leq 0.16\text{rad}$

368 These threshold values are obtained by considering the empirical distribution
369 of base-base interactions shown in Figure 2 in *Bottaro et al. (2014)*. Cis/trans
370 orientation is calculated according to the value of the dihedral angle defined by
371 $C1'_i - N1/N9_i - N1/N9_j - C1'_j$, where N1/N9 is used for pyrimidines and purines,
372 respectively.

373 We note that the annotation provided by Barnaba might fail in detecting some
374 interactions, and sometimes differs from other programs. This is due to the fact
375 that for non-Watson-Crick and stacking interactions it is not trivial to define a
376 set of criteria for a rigorous discrete classification *Waleń et al. (2014)*. Typically,
377 these criteria are calibrated to work well for high-resolution structures, but they
378 are not always suitable to describe nearly-formed interactions often observed in
379 molecular simulations.

380 Torsion angles and 3J scalar couplings

381 We use the standard definition of backbone angles, glycosidic χ angle (O4'-C1'-
382 N9-C4 atoms for A/G, O4'-C1'-N1-C2 for C/U) and sugar torsion angles ($v_0 \dots v_4$) as
383 shown in Figures 8 and 9 *Saenger (2013)*. Pseudorotation sugar parameters am-
384 plitude t_m and phase P are calculated as described in *Altona and Sundaralingam*

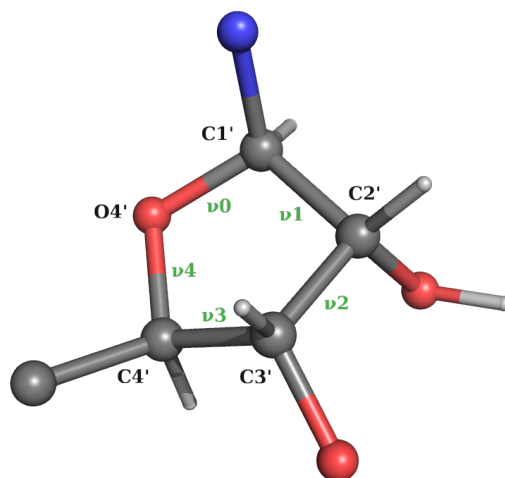


Figure 9. Definition of pucker angles $\nu_0 \dots \nu_4$

385 (1972)

$$P0 = \arctan2(\nu_4 + \nu_1 - \nu_3 - \nu_0, 3.0777\nu_2) \quad (5)$$

$$tm = \nu_2 P0 \quad (6)$$

$$P = \frac{180}{\pi} P0 \quad (7)$$

386 3J Scalar couplings are calculated using the Karplus equations

$$A \cos^2(\theta + \phi) + B \cos(\theta + \phi) + C \quad (8)$$

387 Karplus parameters relative to the different scalar couplings are reported in Table
388 1.

389 Elastic Network Model

390 In ENMs, a set of N beads connected by pairwise harmonic springs penalize
391 deviations of inter-bead distances from their reference values. Spring constants
392 are set to a constant value k whenever the reference distance between the two
393 beads is smaller than an interaction cutoff (R_c), and set to zero otherwise. Under
394 these assumptions, the potential energy of the system can be approximated as

$$U(\delta r_{i,\mu}, \delta r_{j,\nu}) = \delta r_{i,\mu} \mathbf{M}_{ij,\mu\nu} \delta r_{j,\nu} \quad (9)$$

395 where \mathbf{M} is the symmetric $3N \times 3N$ interaction matrix, and $\delta \mathbf{r}_i$ is the deviation of
396 bead i from its position in the reference structure.

397 The user can select different atoms to be used as beads in the construction
398 of the model. The optimal value of the parameter R_c depends on this choice, as
399 described in Ref. *Pinamonti et al. (2015)*.

Table 1. Karplus parameters used in Barnaba

Name	θ	A [Hz]	B [Hz]	C [Hz]	ϕ [rad]	Ref
H1'-H2'	H1'-C1'-C2'-H2'	9.67	-2.03	0	0	<i>Condon et al. (2015)</i>
H2'-H3'	H2'-C2'-C3'-H3'	9.67	-2.03	0	0	<i>Condon et al. (2015)</i>
H3'-H4'	H3'-C3'-C4'-H4'	9.67	-2.03	0	0	<i>Condon et al. (2015)</i>
H5'-P	β	15.3	-6.1	1.6	$-2/3\pi$	<i>Lankhorst et al. (1984)</i>
H5''-P	β	15.3	-6.1	1.6	$2/3\pi$	<i>Lankhorst et al. (1984)</i>
C4-P	β	6.9	-3.4	0.7	0.0	<i>Marino et al. (1999)</i>
H4'-H5'	γ	9.7	-1.8	0.0	$-2/3\pi$	<i>Davies (1978)</i>
H4'-H5''	γ	9.7	-1.8	0.0	0.0	<i>Davies (1978)</i>
H3-P(+1)	ϵ	15.3	-6.1	1.6	$2/3\pi$	<i>Lankhorst et al. (1984)</i>
C4-P(+1)	ϵ	6.9	-3.4	0.7	0.0	<i>Marino et al. (1999)</i>
H1'-C8/C6	χ	4.5	-0.6	0.1	$-\pi/3$	<i>Ippel et al. (1996)</i>
H1'-C4/C2	χ	4.7	2.3	0.1	$-\pi/3$	<i>Ippel et al. (1996)</i>

400 The covariance matrix is computed as

$$C_{ij,\mu\nu} = \sum_{\alpha=6}^{3N} \frac{1}{\lambda_{\alpha}} v_{i,\mu}^{\alpha} v_{j,\nu}^{\alpha} \quad (10)$$

401 Where λ_{α} and v^{α} are the eigenvalues and the eigenvectors of the interaction matrix
402 M , respectively. The sum on α runs over all non-null modes of the system.

403 Mean square fluctuation (MSF) of residue i is calculated as:

$$\text{MSF}_i = \langle \delta r_i^2 \rangle = \sum_{\mu=1}^3 C_{ii,\mu\mu} \quad (11)$$

404 The variance of the distance between two beads can be directly obtained from
405 the covariance matrix in the linear perturbation regime as

$$\sigma_{d_{ij}}^2 = \sum_{\mu,\nu=1}^3 \frac{\tilde{d}_{ij}^{\mu} \tilde{d}_{ij}^{\nu}}{\tilde{d}^2} (C_{ii,\mu\nu} + C_{jj,\mu\nu} - C_{ij,\mu\nu} - C_{ji,\mu\nu}) \quad (12)$$

406 where \tilde{d}_{ij}^{μ} is the μ Cartesian component of the reference distance between bead i
407 and j .

408 For most practical applications of ENMs only the high-amplitude modes, i.e.
409 those with the smallest eigenvalues, provide interesting dynamical information.
410 The calculation of C2-C2 distance fluctuations using Eq. 12 requires the knowledge
411 of all eigenvectors. This can be performed by reducing the system to the "effective
412 interaction matrix" M_{C2}^{eff} relative to the beads of interest *Zen et al. (2008)*.

$$M = \left(\begin{array}{c|c} M_{C2} & W \\ \hline W^T & M_{\text{other}} \end{array} \right) \quad (13)$$

413 Where M_{C2} (M_{other}) is formed by the rows and columns of M relative to the (non)
414 C2 beads, while W represent the interactions between C2 and non-C2 beads. The
415 effective interaction matrix is defined as

$$M_{C2}^{\text{eff}} = M_{C2} - W M_{\text{other}}^{-1} W^T \quad (14)$$

416 This can be computed efficiently using sparse matrix-vector multiplication algo-
417 rithms. The resulting effective matrix M_{C2}^{eff} has reduced size (1/3 for SBP-ENM,
418 1/20 for AA-ENM) making its pseudo-inversion considerably faster. Note that, in
419 case one is interested in computing the C2-C2 fluctuations for a portion of the
420 molecule only, the algorithm could be further optimized by directly computing
421 the effective interactions matrix associated to the required C2-C2 pairs.

422 Acknowledgments

423 We thank D.E Shaw Research for providing the simulation of the UUCG tetraloop.
424 The research is funded by a grant from The Velux Foundations (S.B. and K.L.-
425 L.), a Hallas-Møller Stipend from the Novo Nordisk Foundation (K.L.-L.), and the
426 Lundbeck Foundation BRAINSTRUC initiative (K.L.-L.). G.B., S.R, S.B and G.P. have
427 received funding from the European Research Council (ERC) under the European
428 Union's Seventh Framework Programme (FP/2007-2013)/ERC grant agreement
429 no. 306662 (S-RNA-S). W.B. is funded from VILLUM FONDEN (VKR023445) and the
430 Danish Council for Independent Research (DFF-4181-00344).

431 References

- 432 **Abraham MJ**, Murtola T, Schulz R, Páll S, Smith JC, Hess B, Lindahl E. GROMACS: High
433 performance molecular simulations through multi-level parallelism from laptops to
434 supercomputers. *SoftwareX*. 2015; 1:19–25.
- 435 **Altona Ct**, Sundaralingam M. Conformational analysis of the sugar ring in nucleosides
436 and nucleotides. New description using the concept of pseudorotation. *Journal of the*
437 *American Chemical Society*. 1972; 94(23):8205–8212.
- 438 **Bahar I**, Jernigan RL. Vibrational dynamics of transfer RNAs: comparison of the free and
439 synthetase-bound forms. *The Journal of Molecular Biology*. 1998; 281(5):871–884.
- 440 **Bottaro S**, Banas P, Sponer J, Bussi G. Free Energy Landscape of GAGA and UUCG RNA
441 Tetraloops. *J Phys Chem Lett*. 2016; 7(20):4032–4038.
- 442 **Bottaro S**, Bussi G, Kennedy SD, Turner DH, Lindorff-Larsen K. Conformational ensembles
443 of RNA oligonucleotides from integrating NMR and molecular simulations. *Science*
444 *Advances*. 2018; 4(5):eaar8521.
- 445 **Bottaro S**, Di Palma F, Bussi G. The role of nucleobase interactions in RNA structure and
446 dynamics. *Nucleic Acids Res*. 2014; 42(21):13306–13314.

- 447 **Bottaro S**, Lindorff-Larsen K. Mapping the universe of RNA tetraloop folds. *Biophys J.*
448 2017; 113(2):257–267.
- 449 **Chen H**, Meisburger SP, Pabit SA, Sutton JL, Webb WW, Pollack L. Ionic strength-dependent
450 persistence lengths of single-stranded RNA and DNA. *Proceedings of the National*
451 *Academy of Sciences.* 2012; 109(3):799–804.
- 452 **Condon DE**, Kennedy SD, Mort BC, Kierzek R, Yildirim I, Turner DH. Stacking in RNA:
453 NMR of four tetramers benchmark molecular dynamics. *J Chem Theor Comput.* 2015;
454 11(6):2729–2742.
- 455 **Davies DB.** Conformations of nucleosides and nucleotides. *Prog Nucl Magn Reson*
456 *Spectrosc.* 1978; 12(3):135–225.
- 457 **Dawson WK**, Bujnicki JM. Computational modeling of RNA 3D structures and interactions.
458 *Current opinion in structural biology.* 2016; 37:22–28.
- 459 **Dickerson R.** Definitions and nomenclature of nucleic acid structure components. *Nucleic*
460 *acids research.* 1989; 17(5):1797–1803.
- 461 **Ester M**, Kriegel HP, Sander J, Xu X, et al. A density-based algorithm for discovering clusters
462 in large spatial databases with noise. In: *Kdd*, vol. 96; 1996. p. 226–231.
- 463 **Frellsen J**, Moltke I, Thiim M, Mardia K, Ferkinghoff-Borg J, Hamelryck T. A Probabilistic
464 Model of RNA Conformational Space. *PLoS Comput Biol.* 2009; 5(3):e1000406.
- 465 **Gendron P**, Lemieux S, Major F. Quantitative analysis of nucleic acid three-dimensional
466 structures. *Journal of molecular biology.* 2001; 308(5):919–936.
- 467 **Górska A**, Jasiński M, Trylska J. MINT: software to identify motifs and short-range interac-
468 tions in trajectories of nucleic acids. *Nucleic acids research.* 2015; 43(17):e114–e114.
- 469 **Hajdin CE**, Bellaousov S, Huggins W, Leonard CW, Mathews DH, Weeks KM. Accurate
470 SHAPE-directed RNA secondary structure modeling, including pseudoknots. *Proc Natl*
471 *Acad Sci.* 2013; 110(14):5498–5503.
- 472 **Ippel J**, Wijmenga S, De Jong R, Heus H, Hilbers C, De Vroom E, Van der Marel G, Van Boom
473 J. Heteronuclear scalar couplings in the bases and sugar rings of nucleic acids: their
474 determination and application in assignment and conformational analysis. *Magn Reson*
475 *Chem.* 1996; 34(13):S156–S176.
- 476 **Jacobson AB**, Zuker M. Structural analysis by energy dot plot of a large mRNA. *Journal of*
477 *molecular biology.* 1993; 233(2):261–269.
- 478 **Kabsch W.** A solution for the best rotation to relate two sets of vectors. *Acta Crystallo-*
479 *graphica Section A: Crystal Physics, Diffraction, Theoretical and General Crystallography.*
480 1976; 32(5):922–923.
- 481 **Kuhrova P**, Best RB, Bottaro S, Bussi G, Sponer J, Otyepka M, Banas P. Computer folding
482 of RNA tetraloops: identification of key force field deficiencies. *Journal of chemical*
483 *theory and computation.* 2016; 12(9):4534–4548.

- 484 **Kumar R**, Grubmüller H. do_x3dna: a tool to analyze structural fluctuations of dsDNA or
485 dsRNA from molecular dynamics simulations. *Bioinformatics*. 2015; 31(15):2583–2585.
- 486 **Lankhorst PP**, Haasnoot CA, Erkelens C, Altona C. Carbon-13 NMR in conformational
487 analysis of nucleic acid fragments 2. A reparametrization of the Karplus equation for
488 vicinal NMR coupling constants in CCOP and HCOP fragments. *J Biomol Struct Dyn*.
489 1984; 1(6):1387–1405.
- 490 **Lavery R**, Moakher M, Maddocks JH, Petkeviciute D, Zakrzewska K. Conformational
491 analysis of nucleic acids revisited: Curves+. *Nucleic acids research*. 2009; 37(17):5917–
492 5929.
- 493 **Lemieux S**, Major F. RNA canonical and non-canonical base pairing types: a recognition
494 method and complete repertoire. *Nucleic acids research*. 2002; 30(19):4250–4263.
- 495 **Leontis NB**, Westhof E. Geometric nomenclature and classification of RNA base pairs.
496 *Rna*. 2001; 7(4):499–512.
- 497 **Lu XJ**, Bussemaker HJ, Olson WK. DSSR: an integrated software tool for dissecting the
498 spatial structure of RNA. *Nucleic acids research*. 2015; 43(21):e142–e142.
- 499 **Lu XJ**, Olson WK. 3DNA: a versatile, integrated software system for the analysis, rebuilding
500 and visualization of three-dimensional nucleic-acid structures. *Nature protocols*. 2008;
501 3(7):1213–1227.
- 502 **Marino JP**, Schwalbe H, Griesinger C. J-coupling restraints in RNA structure determination.
503 *Acc Chem Res*. 1999; 32(7):614–623.
- 504 **McGibbon RT**, Beauchamp KA, Harrigan MP, Klein C, Swails JM, Hernández CX, Schwantes
505 CR, Wang LP, Lane TJ, Pande VS. MDTraj: A Modern Open Library for the Analysis of
506 Molecular Dynamics Trajectories. *Biophysical Journal*. 2015; 109(8):1528 – 1532. doi:
507 [10.1016/j.bpj.2015.08.015](https://doi.org/10.1016/j.bpj.2015.08.015).
- 508 **Merino EJ**, Wilkinson KA, Coughlan JL, Weeks KM. RNA structure analysis at single nu-
509 cleotide resolution by selective 2'-hydroxyl acylation and primer extension (SHAPE).
510 *Journal of the American Chemical Society*. 2005; 127(12):4223–4231.
- 511 **Miao Z**, Adamiak RW, Antczak M, Batey RT, Becka AJ, Biesiada M, Boniecki MJ, Bujnicki JM,
512 Chen SJ, Cheng CY, et al. RNA-Puzzles Round III: 3D RNA structure prediction of five
513 riboswitches and one ribozyme. *RNA*. 2017; 23(5):655–672.
- 514 **Michaud-Agrawal N**, Denning EJ, Woolf TB, Beckstein O. MDAnalysis: a toolkit for the
515 analysis of molecular dynamics simulations. *Journal of computational chemistry*. 2011;
516 32(10):2319–2327.
- 517 **Nozinovic S**, Fürtig B, Jonker HR, Richter C, Schwalbe H. High-resolution NMR structure of
518 an RNA model system: the 14-mer cUUCGg tetraloop hairpin RNA. *Nucleic Acids Res*.
519 2010; 38(2):683–694.
- 520 **Parisien M**, Cruz JA, Westhof É, Major F. New metrics for comparing and assessing
521 discrepancies between RNA 3D structures and models. *Rna*. 2009; 15(10):1875–1885.

- 522 **Pinamonti G**, Bottaro S, Micheletti C, Bussi G. Elastic network models for RNA: a com-
523 parative assessment with molecular dynamics and SHAPE experiments. *Nucleic acids*
524 *research*. 2015; 43(15):7260–7269.
- 525 **Pinamonti G**, Zhao J, Condon DE, Paul F, Noé F, Turner DH, Bussi G. Predicting the kinetics
526 of RNA oligonucleotides using Markov state models. *Journal of chemical theory and*
527 *computation*. 2017; 13(2):926–934.
- 528 **Poblete S**, Bottaro S, Bussi G. A nucleobase-centered coarse-grained representation for
529 structure prediction of RNA motifs. *Nucleic Acids Research*. 2018; 46:1674.
- 530 **Richardson JS**, Schneider B, Murray LW, Kapral GJ, Immormino RM, Headd JJ, Richardson
531 DC, Ham D, Hershkovits E, Williams LD, et al. RNA backbone: consensus all-angle con-
532 formers and modular string nomenclature (an RNA Ontology Consortium contribution).
533 *Rna*. 2008; 14(3):465–481.
- 534 **Roe DR**, Cheatham III TE. PTRAJ and CPPTRAJ: software for processing and analysis of
535 molecular dynamics trajectory data. *Journal of chemical theory and computation*. 2013;
536 9(7):3084–3095.
- 537 **Saenger W**. Principles of nucleic acid structure. Springer Science & Business Media; 2013.
- 538 **Sarver M**, Zirbel CL, Stombaugh J, Mokdad A, Leontis NB. FR3D: finding local and compos-
539 ite recurrent structural motifs in RNA 3D structures. *Journal of mathematical biology*.
540 2008; 56(1-2):215–252.
- 541 **Setny P**, Zacharias M. Elastic Network Models of Nucleic Acids Flexibility. *Journal of*
542 *Chemical Theory and Computation*. 2013; 9(12):5460–5470.
- 543 **Šponer J**, Bussi G, Krepl M, Banáš P, Bottaro S, Cunha RA, Gil-Ley A, Pinamonti G, Poblete
544 S, Jurečka P, Walter NG, Otyepka M. RNA Structural Dynamics As Captured by Molecular
545 Simulations: A Comprehensive Overview. *Chem Rev*. 2018; 118:4177.
- 546 **Tan D**, Piana S, Dirks RM, Shaw DE. RNA force field with accuracy comparable to state-of-
547 the-art protein force fields. *Proceedings of the National Academy of Sciences*. 2018; p.
548 201713027.
- 549 **Tiberti M**, Papaleo E, Bengtsen T, Boomsma W, Lindorff-Larsen K. ENCORE: soft-
550 ware for quantitative ensemble comparison. *PLoS computational biology*. 2015;
551 11(10):e1004415.
- 552 **Tirion MM**. Large amplitude elastic motions in proteins from a single-parameter, atomic
553 analysis. *Phys Rev Lett*. 1996; 77(9):1905.
- 554 **Tribello GA**, Bonomi M, Branduardi D, Camilloni C, Bussi G. PLUMED 2: New feathers for
555 an old bird. *Computer Physics Communications*. 2014; 185(2):604–613.
- 556 **Waleń T**, Chojnowski G, Gierski P, Bujnicki JM. ClaRNA: a classifier of contacts in RNA 3D
557 structures based on a comparative analysis of various classification schemes. *Nucleic*
558 *acids research*. 2014; 42(19):e151–e151.

- 559 **Yang C**, Lim M, Kim E, Pak Y. Predicting RNA structures via a simple van der Waals
560 correction to an all-atom force field. *Journal of chemical theory and computation*. 2017;
561 13(2):395–399.
- 562 **Zen A**, Carnevale V, Lesk AM, Micheletti C. Correspondences between low-energy modes
563 in enzymes: Dynamics-based alignment of enzymatic functional families. *Protein*
564 *Science*. 2008; 17(5):918–929.
- 565 **Zimmermann MT**, Jernigan RL. Elastic network models capture the motions apparent
566 within ensembles of RNA structures. *RNA*. 2014; 20(6):792–804.